

Windowing Techniques in Frequency-Domain Simulation

Giorgio Casinovi

School of Electrical and Computer Engineering
Georgia Institute of Technology
Atlanta, GA 30332-0250

Abstract

The verification of a number of mixed-technology and mixed-signal designs (RF circuits, for instance) often requires frequency-domain simulations of nonlinear systems in the presence of signals that are best characterized as having continuous frequency spectra. This paper describes a new frequency-domain simulation algorithm for the computation of the response of nonlinear systems to band-limited signals with continuous spectra. The algorithm is based on an orthogonal series expansion of the signals in the frequency domain, and does not rely on a linearization of the system equations. Signal spectra are obtained from the solution of a system of nonlinear algebraic equations, and windowing techniques are used to eliminate the Gibbs phenomenon and to improve the spectral accuracy of the results. For this purpose, the performance of a number of windows is compared on the basis of a newly introduced characteristic function, the windowing error kernel. Numerical results obtained from the simulation of an optical amplifier that are representative of the algorithm's performance are presented.

Introduction

Recent technological advances in a number of areas (MEMS and wireless communications, for instance) have renewed the interest in the development of algorithms and tools for the verification of mixed-signal and mixed-technology designs. Among them, frequency-domain simulation methods have acquired increased importance, because they are often better suited to assess the performance of particular types of systems, such as RF circuits [1].

Most frequency-domain analysis methods developed so far [2, 3, 4, 5] are based, either explicitly or implicitly, on a linearization of the system equations. Hence they cannot be used in those cases where the nonlinearities in the system response cannot be ignored.

The only existing frequency-domain simulation methods that can fully handle nonlinearities rely on the principle of harmonic balance [6], and a number of algorithms based on this approach have been published [7, 8]. In harmonic balance, the solution to the system equations is expressed as a periodic or quasi-periodic Fourier series in the time domain. The drawback intrinsic in this approach is that, by construction, it can only handle signals with discrete frequency spectra. There are many situations, however, in which it is necessary to simulate the behavior of a system in the presence of signals that do not satisfy this requirement. For instance, the successful design of mixed-signal integrated circuits, in which analog and digital components are fabricated on the same chip, requires the assessment of the impact of digital noise on the performance of the analog portions of the system. The noise generated by digital circuits is best characterized as having a continuous frequency spectrum.

This paper presents a new frequency-domain simulation algorithm developed specifically to compute the response of nonlinear systems to band-limited signals having continuous spectra. The algorithm is based on a truncated Fourier series expansion of the signals in the frequency domain. Thus it can be considered, in a sense, the dual approach to frequency-domain simulation with respect to harmonic balance. Windowing techniques are used to eliminate spurious oscillations in the computed spectrum caused by the Gibbs phenomenon. A quantitative comparison of various windows is presented, based on a newly introduced function associated with the window, named the *windowing error kernel*. Results obtained from numerical simulations with and without windowing are compared.

Nonlinear frequency-domain simulation

Consider a nonlinear system (e.g. an integrated circuit) that is described by the following system of equations:

$$\frac{d}{dt}\mathbf{f}[\mathbf{x}(t), t] + \mathbf{g}[\mathbf{x}(t), t] = \mathbf{u}(t). \quad (1)$$

This work was supported in part by DARPA under contract F33615-01-C-1971.

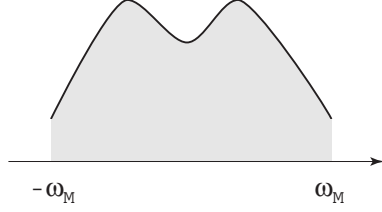


Fig. 1. Continuous frequency spectrum

In addition to lumped-constant electrical networks, this equation describes many other types of dynamical systems, with the variables taking on various physical meanings.

In the frequency domain, equation (1) can be expressed as [6]:

$$j\omega\mathbf{F}[\mathbf{X}(\omega)] + \mathbf{G}[\mathbf{X}(\omega)] = \mathbf{U}(\omega), \quad (2)$$

where $\mathbf{X}(\omega)$ and $\mathbf{U}(\omega)$ represent the Fourier transforms of $\mathbf{x}(t)$ and $\mathbf{u}(t)$. The traditional approaches to frequency-domain analysis, which are based on harmonic balance, perform sinusoidal expansions of the signals in the time domain. This type of expansion, however, is applicable only to signals that have discrete spectra. It will now be shown that a dual approach, based on a sinusoidal expansion of the signals *in the frequency domain*, can be used to solve (1) (or, equivalently, (2)) when the signals involved have continuous spectra.

It will be assumed that both the input $\mathbf{u}(t)$ and the solution $\mathbf{x}(t)$ have a frequency spectrum that has a finite upper bound ω_M , as shown in Fig. 1. In practice, this condition can always be satisfied by choosing ω_M sufficiently large. Moreover, it will also be assumed that the spectra of $\mathbf{f}[\mathbf{x}(t), t]$ and $\mathbf{g}[\mathbf{x}(t), t]$ satisfy the same condition.

In many instances, $\mathbf{u}(t)$ and $\mathbf{x}(t)$ contain a DC component, which creates a spike¹ in their spectra at $\omega = 0$. The presence of spikes makes it problematic from a numerical standpoint to obtain an orthogonal series expansion of the spectrum. For this reason, it is more convenient to rewrite (1) so that the DC component is separated from the signals. For this purpose, let \mathbf{u}_0 , \mathbf{x}_0 , \mathbf{f}_0 and \mathbf{g}_0 be the DC components of $\mathbf{u}(t)$, $\mathbf{x}(t)$, $\mathbf{f}[\mathbf{x}(t), t]$ and $\mathbf{g}[\mathbf{x}(t), t]$, respectively, and define the following quantities:

$$\begin{aligned} \Delta\mathbf{x}(t) &= \mathbf{x}(t) - \mathbf{x}_0, \\ \Delta\mathbf{u}(t) &= \mathbf{u}(t) - \mathbf{u}_0, \\ \Delta\mathbf{f}[\Delta\mathbf{x}(t), t] &= \mathbf{f}[\mathbf{x}_0 + \Delta\mathbf{x}(t), t] - \mathbf{f}_0, \\ \Delta\mathbf{g}[\Delta\mathbf{x}(t), t] &= \mathbf{g}[\mathbf{x}_0 + \Delta\mathbf{x}(t), t] - \mathbf{g}_0. \end{aligned}$$

Since $\mathbf{u}_0 = \mathbf{U}(0)$ and $\mathbf{g}_0 = \mathbf{G}[\mathbf{X}(0)]$, setting $\omega = 0$ in (2)

¹Theoretically, a Dirac impulse.

shows that $\mathbf{g}_0 = \mathbf{u}_0$. Therefore the following equation is equivalent to (1):

$$\frac{d}{dt}\Delta\mathbf{f}[\Delta\mathbf{x}(t), t] + \Delta\mathbf{g}[\Delta\mathbf{x}(t), t] = \Delta\mathbf{u}(t). \quad (3)$$

Note that this is *not* a linearization of (1) around the DC component of the signals: it is easy to verify that $\mathbf{x}(t) = \mathbf{x}_0 + \Delta\mathbf{x}(t)$ solves (1) exactly, if $\Delta\mathbf{x}(t)$ is the solution of (3).

By assumption, the spectra of all the terms in (3) are contained in the interval $[-\omega_M, \omega_M]$. Therefore they can be expanded in an orthogonal series over that interval. For example:

$$\Delta\mathbf{U}(\omega) = \sum_{k=-\infty}^{\infty} \mathbf{U}_{-k} e^{-jk\hat{\omega}} r_{\pi}(\hat{\omega}), \quad (4)$$

where $\hat{\omega} = \pi\omega/\omega_M$ and $r_{\pi}(\hat{\omega})$ is defined as:

$$r_{\pi}(\hat{\omega}) = \begin{cases} 1, & |\hat{\omega}| \leq \pi \\ 0, & |\hat{\omega}| > \pi. \end{cases}$$

Taking the inverse Fourier transform of (4) yields the following series expansion for $\Delta\mathbf{u}(t)$:

$$\Delta\mathbf{u}(t) = \frac{\omega_M}{\pi} \sum_{k=-\infty}^{\infty} \mathbf{U}_{-k} \text{sinc}[\omega_M(t - t_k)/\pi], \quad (5)$$

where: $\text{sinc } x = \sin \pi x / (\pi x)$, and $t_k = k\pi/\omega_M$. Evaluating this expression at $t = t_n$ shows that coefficients \mathbf{U}_k in (4) are related to the values of $\Delta\mathbf{u}(t)$ by the following relationship:

$$\Delta\mathbf{u}(t_n) = \frac{\omega_M}{\pi} \mathbf{U}_{-n}. \quad (6)$$

Equations (5) and (6), taken together, express the well-known sampling theorem [9].

A similar series expansion can be obtained for the left-hand side of (3):

$$\begin{aligned} \frac{d}{dt}\Delta\mathbf{f}[\Delta\mathbf{x}(t), t] + \Delta\mathbf{g}[\Delta\mathbf{x}(t), t] \\ = \sum_{k=-\infty}^{\infty} \left(\Delta\dot{\mathbf{f}}[\Delta\mathbf{x}(t_k), t_k] + \Delta\mathbf{g}[\Delta\mathbf{x}(t_k), t_k] \right) \cdot \\ \text{sinc}[\omega_M(t - t_k)/\pi], \end{aligned}$$

where: $\Delta\dot{\mathbf{f}}[\Delta\mathbf{x}(t_k), t_k] = \left. \frac{d}{dt}\Delta\mathbf{f}[\Delta\mathbf{x}(t), t] \right|_{t=t_k}$. Consequently, in order for (3) to be satisfied the following equality must hold at all points t_k :

$$\Delta\dot{\mathbf{f}}[\Delta\mathbf{x}(t_k), t_k] + \Delta\mathbf{g}[\Delta\mathbf{x}(t_k), t_k] = \Delta\mathbf{u}(t_k). \quad (7)$$

An expression for $\Delta\dot{\mathbf{f}}[\mathbf{x}(t_k), t_k]$ can be obtained starting from the following series expansion:

$$\Delta\mathbf{f}[\Delta\mathbf{x}(t), t] = \sum_{i=-\infty}^{\infty} \Delta\mathbf{f}[\Delta\mathbf{x}(t_i), t_i] \text{sinc}[\omega_M(t - t_i)/\pi].$$

Differentiating both sides of this equation yields:

$$\begin{aligned} \Delta \dot{\mathbf{f}}[\Delta \mathbf{x}(t_k), t_k] \\ = \frac{\omega_M}{\pi} \sum_{i=-\infty}^{\infty} \Delta \mathbf{f}[\Delta \mathbf{x}(t_i), t_i] \text{sinc}'[\omega_M(t_k - t_i)/\pi]. \end{aligned}$$

But:

$$\begin{aligned} \text{sinc}'[\omega_M(t_k - t_i)/\pi] &= \text{sinc}'(k - i) \\ &= \begin{cases} 0, & i = k \\ \frac{(-1)^{k-i}}{(k-i)}, & i \neq k. \end{cases} \end{aligned}$$

Therefore:

$$\Delta \dot{\mathbf{f}}[\Delta \mathbf{x}(t_k), t_k] = \frac{\omega_M}{\pi} \sum_{\substack{i=-\infty \\ i \neq k}}^{\infty} \Delta \mathbf{f}[\Delta \mathbf{x}(t_i), t_i] \frac{(-1)^{k-i}}{k-i}, \quad (8)$$

where the value $i = k$ is excluded from the summation. Substituting this expression for $\Delta \dot{\mathbf{f}}[\Delta \mathbf{x}(t_k), t_k]$ in (7), and truncating the infinite series to a finite number of terms (which is dependent upon the accuracy that one wishes to achieve), yields the following equation:

$$\begin{aligned} \frac{\omega_M}{\pi} \sum_{\substack{i=-N \\ i \neq k}}^N \Delta \mathbf{f}[\Delta \mathbf{x}(t_i), t_i] \frac{(-1)^{k-i}}{k-i} \\ + \Delta \mathbf{g}[\Delta \mathbf{x}(t_k), t_k] = \Delta \mathbf{u}(t_k). \quad (9) \end{aligned}$$

This is a set of $2N + 1$ algebraic equations in the $2N + 1$ unknowns $\Delta \mathbf{x}(t_{-N}), \Delta \mathbf{x}(t_{-N+1}), \dots, \Delta \mathbf{x}(t_N)$, which can be solved using Newton's method. The spectrum of $\Delta \mathbf{x}(t)$ can then be computed from relationships analogous to those in (4) and (6):

$$\Delta \mathbf{X}_N(\omega) = \frac{\pi}{\omega_M} \sum_{k=-N}^N \Delta \mathbf{x}(t_k) e^{-jk\hat{\omega}} r_{\pi}(\hat{\omega}). \quad (10)$$

As an example, consider a simple first-order low-pass *RC* circuit with a 3-dB frequency of 128 kHz and an input signal with a uniform frequency spectrum between -512 kHz and 512 kHz (white noise). If this circuit is simulated using the algorithm described above, the spectrum of the output signal, as given by (10) with $N = 128$, is shown in Fig. 2. While its overall shape matches that of the filter's transfer function, as expected, a spurious superimposed oscillation is also clearly visible in the graph. This is a well-known effect, which is caused by the abrupt truncation of an infinitely long signal to one of finite length (Gibbs phenomenon). One way to reduce or eliminate this unwanted effect is to use windowing techniques [10].

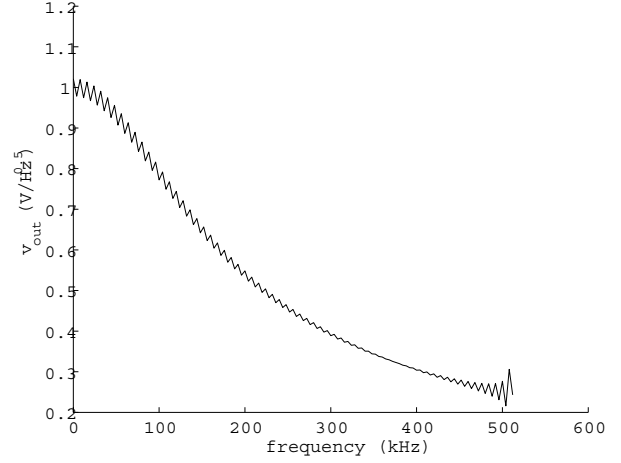


Fig. 2. Output spectrum of RC low-pass filter

Windowing

Given a sequence $\{x_k\}$, finite or infinite, its Discrete Fourier Transform (DFT) is defined as:

$$X(\hat{\omega}) = \sum_{k=-\infty}^{+\infty} x_k e^{-jk\hat{\omega}}. \quad (11)$$

The technique known as *windowing* consists of multiplying term-by-term the sequence $\{x_k\}$ by a finite sequence of weights $\{w_k\}$ before computing the DFT:

$$X_W(\hat{\omega}) = \sum_{k=-N}^N w_k x_k e^{-jk\hat{\omega}}. \quad (12)$$

Truncation of the infinite series in (11) to a finite number of terms is a special case of windowing, corresponding to $w_{-N} = w_{-N+1} = \dots = w_N = 1$; this particular choice of weights is known as the *rectangular window*.

A comparison of (10) with (12) shows that, for $\omega \in [-\omega_M, \omega_M]$, $\Delta \mathbf{X}_N(\omega) = (\pi/\omega_M) X_W(\hat{\omega})$, where $X_W(\hat{\omega})$ is obtained by applying the rectangular window to the theoretically infinite sequence $x_k = \Delta \mathbf{x}(t_k)$. It will be shown in the remainder of this section that using other windows to compute $\Delta \mathbf{X}_N(\omega)$ leads to a significant improvement in the simulation results.

A well-known theorem of Fourier analysis [9] states that:

$$X_W(\hat{\omega}) = \frac{1}{2\pi} X(\hat{\omega}) * W(\hat{\omega}) = \frac{1}{2\pi} \int_{-\pi}^{\pi} X(\theta) W(\hat{\omega} - \theta) d\theta,$$

where $W(\hat{\omega})$ is the DFT of $\{w_k\}$:

$$W(\hat{\omega}) = \sum_{k=-N}^N w_k e^{-jk\hat{\omega}}.$$

Let:

$$I_W(\hat{\omega}) = \frac{w_0}{2\pi} \hat{\omega} + j \sum_{\substack{k=-N \\ k \neq 0}}^N \frac{w_k}{2\pi k} e^{-jk\hat{\omega}}.$$

Then:

$$\begin{aligned} X_W(\hat{\omega}) &= X(-\pi)I_W(\hat{\omega} + \pi) - X(\pi)I_W(\hat{\omega} - \pi) \\ &\quad + \int_{-\pi}^{\pi} X'(\theta)I_W(\hat{\omega} - \theta) d\theta. \end{aligned}$$

Furthermore, it is easy to verify that:

$$X(\hat{\omega}) = \frac{X(-\pi) + X(\pi)}{2} + \frac{1}{2} \int_{-\pi}^{\pi} X'(\theta) \text{sign}(\hat{\omega} - \theta) d\theta.$$

Therefore the difference between $X_W(\hat{\omega})$ and $X(\hat{\omega})$ is given by:

$$\begin{aligned} E_W(\hat{\omega}) &= X_W(\hat{\omega}) - X(\hat{\omega}) \\ &= X(-\pi)[I_W(\hat{\omega} + \pi) - \frac{1}{2}] \\ &\quad - X(\pi)[I_W(\hat{\omega} - \pi) + \frac{1}{2}] \\ &\quad + \int_{-\pi}^{\pi} X'(\theta)K_W(\hat{\omega} - \theta) d\theta, \quad (13) \end{aligned}$$

where $K(\hat{\omega}) = I_W(\hat{\omega}) - 1/2 \text{sign}(\hat{\omega})$. $E_W(\hat{\omega})$ represents the error introduced by windowing in the computation of the DFT.

Equation (13) can be simplified if $w_0 = 1$. This condition is satisfied by all windows that are used in practice, because it ensures that $E_W(\hat{\omega}) = 0$ whenever $X(\hat{\omega})$ is a constant. Assuming $w_0 = 1$, the following equalities hold:

$$I_W(\hat{\omega} + \pi) - \frac{1}{2} = I_W(\hat{\omega} - \pi) + \frac{1}{2} = K_W(\hat{\omega} - \pi),$$

and (13) becomes:

$$\begin{aligned} E_W(\hat{\omega}) &= [X(-\pi) - X(\pi)]K_W(\hat{\omega} - \pi) \\ &\quad + \int_{-\pi}^{\pi} X'(\theta)K_W(\hat{\omega} - \theta) d\theta. \quad (14) \end{aligned}$$

The last term on the right-hand side of this equation is the convolution of $X'(\hat{\omega})$, the derivative of the DFT of the original sequence, with $K_W(\hat{\omega})$, a function that depends on the window used. If $X(\hat{\omega})$ has a discontinuity at $\hat{\omega}_0$, then: $X'(\hat{\omega}_0) = [X(\hat{\omega}_0^+) - X(\hat{\omega}_0^-)]\delta(\hat{\omega} - \hat{\omega}_0)$. The presence of this Dirac impulse in the convolution integral generates a term equal to $[X(\hat{\omega}_0^+) - X(\hat{\omega}_0^-)]K_W(\hat{\omega} - \hat{\omega}_0)$ in the expression for $E_W(\hat{\omega})$.

If $X(\hat{\omega})$ is considered to be a periodic function of period 2π , then: $X(\pi^+) = X(-\pi)$. This allows the first term on the right-hand side of (14) to be interpreted as the result

of a discontinuity in $X(\hat{\omega})$ at $\hat{\omega}_0 = \pi$. Thus (14) can be rewritten simply as:

$$E_W(\hat{\omega}) = \oint_{2\pi} X'(\theta)K_W(\hat{\omega} - \theta) d\theta, \quad (15)$$

with the understanding that $X(\hat{\omega})$ must be regarded as a periodic function of period 2π , and that discontinuities in $X(\hat{\omega})$ (including at $\hat{\omega} = \pi$) generate Dirac impulses in $X'(\hat{\omega})$, as explained above. Equation (15) shows that the error introduced by windowing is completely characterized by $K_W(\hat{\omega})$; for this reason, $K_W(\hat{\omega})$ will be referred to as the *windowing error kernel*.

In particular, the presence or absence of oscillations in $K_W(\hat{\omega})$ gives a good indication of the presence or absence of oscillations in $E_W(\hat{\omega})$, as can be seen by approximating the integral in (15) with a finite sum:

$$E_W(\hat{\omega}) \approx \sum_i \Delta\theta_i X'(\theta_i)K_W(\hat{\omega} - \theta_i).$$

This approximate equality shows that $E_W(\hat{\omega})$ can be thought of as the sum of shifted and scaled copies of $K_W(\hat{\omega})$.

All windows that are used in practice are real and symmetric ($w_{-k} = w_k$). In this case, both $I_W(\hat{\omega})$ and $K_W(\hat{\omega})$ are odd functions, $I_W(0) = 0$, and $K(0^-) = -K(0^+) = 1/2$. The five windows listed below are among those most frequently mentioned in the literature [9, 10]:

Rectangular:

$$w_k = 1, \quad k = -N, \dots, N.$$

Bartlett:

$$w_k = 1 - |k|/N, \quad k = -N, \dots, N.$$

Hanning:

$$w_k = [1 + \cos(k\pi/N)]/2, \quad k = -N, \dots, N.$$

Hamming:

$$w_k = 0.54 + 0.46 \cos(k\pi/N), \quad k = -N, \dots, N.$$

Blackmann:

$$w_k = 0.42 + 0.5 \cos(k\pi/N) + 0.08 \cos(2k\pi/N), \quad k = -N, \dots, N.$$

For comparison purposes, Fig. 3 shows the graphs of $K_W(\hat{\omega})$, with $N = 8$, for four of them (the graph for the Hamming window is not shown because it is difficult to distinguish it from the graph of the Hanning window in that figure). As a first observation, the pronounced oscillations in the rectangular window's graph are absent

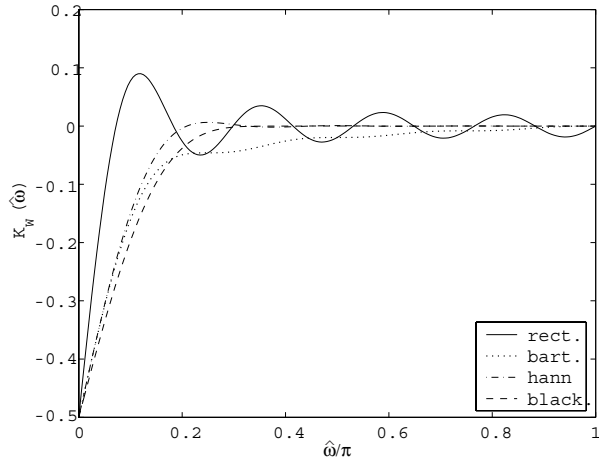


Fig. 3. Windowing error kernels for $N = 8$

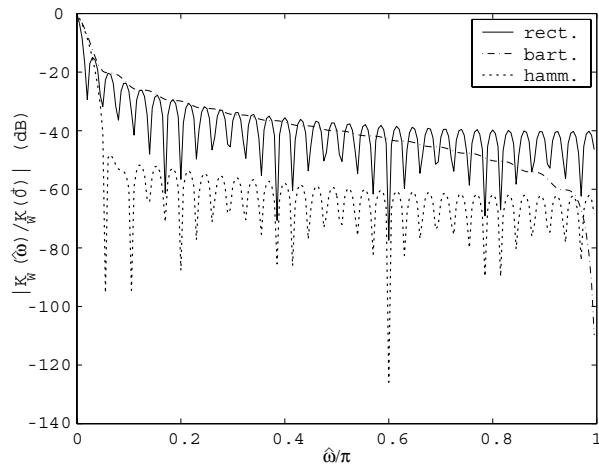


Fig. 4. Normalized windowing error kernel, $N = 32$

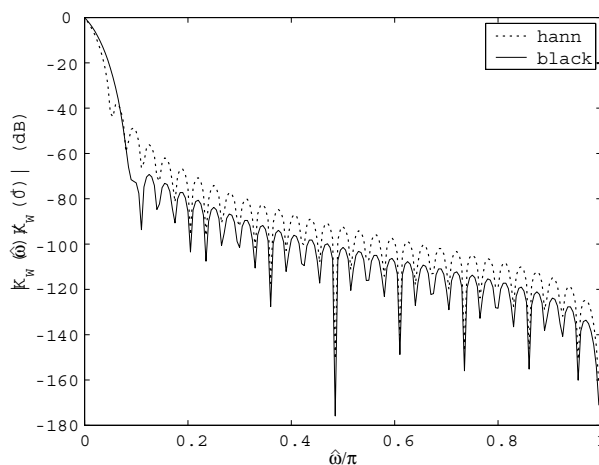


Fig. 5. Normalized windowing error kernel, $N = 32$

from all the other graphs, indicating that the other four windows will generate smoother approximations to $X(\hat{\omega})$.

	-20 dB		
	$N = 16$	$N = 32$	$N = 64$
Bartlett	10.4	5.27	2.65
Hanning	7.49	3.75	1.87
Hamming	7.13	3.56	1.78
Blackmann	9.35	4.67	2.34
	-40 dB		
	$N = 16$	$N = 32$	$N = 64$
Bartlett	69.6	48.9	29.5
Hanning	13.8	6.89	3.45
Hamming	10.0	4.97	2.48
Blackmann	13.7	6.84	3.42

Table 1. Values of $\hat{\omega}/\pi$ (in percent) at specified error kernel attenuations

Furthermore, the rate at which $|K_W(\hat{\omega})|$ decays as $|\hat{\omega}|$ increases provides a way to compare the relative accuracy of the various windows. For this purpose, Figs. 4 and 5 show the graphs of $|K_W(\hat{\omega})/K_W(0^+)|$, on logarithmic scale, for the five windows listed above with $N = 32$. An examination of those figures shows that, despite the absence of oscillations, the Bartlett window is not likely to produce more accurate results than the rectangular window, as the corresponding graphs decay at very similar rates. The Hamming window's kernel instead falls 40 dB below its peak value at $\hat{\omega} \approx 0.1\pi$, indicating that two features (e.g. two peaks) in $X(\hat{\omega})$ that are separated by 40 dB or less are likely to be visible in $X_W(\hat{\omega})$, provided that their distance is at least 10% of ω_M . The graph, however, never decreases below a floor of approximately 50 dB, which means that this window's separation resolution is at most 50 dB, and perhaps less. On the other hand, the amplitudes of the side lobes of the Hanning and Blackmann windows keep decreasing well below those of the three other windows, an indication that they can achieve better separation resolution.

One way to quantify the relative accuracy of the various windows is to compute the value of $\hat{\omega}$ where the ratio $|K_W(\hat{\omega})/K_W(0^+)|$ falls below a certain level. Those values (expressed as a fraction of π) are listed in Table 1 for four of the five windows, and for three different values of N . The figures reported in the table show that the performances of the Hanning, Hamming and Blackman windows are essentially equivalent for separation resolutions of 40 dB or less. Figs. 4 and 5, however, show that the Hanning and Blackmann windows can achieve higher resolution separation. In fact, among the five windows considered here the Blackmann window appears to offer the best overall performance.

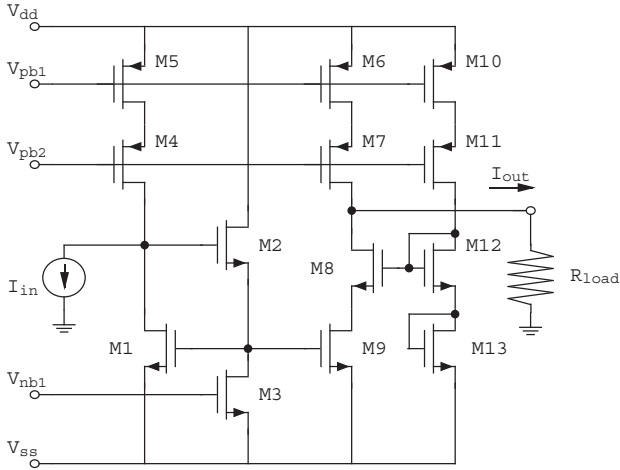


Fig. 6. A CMOS optical amplifier

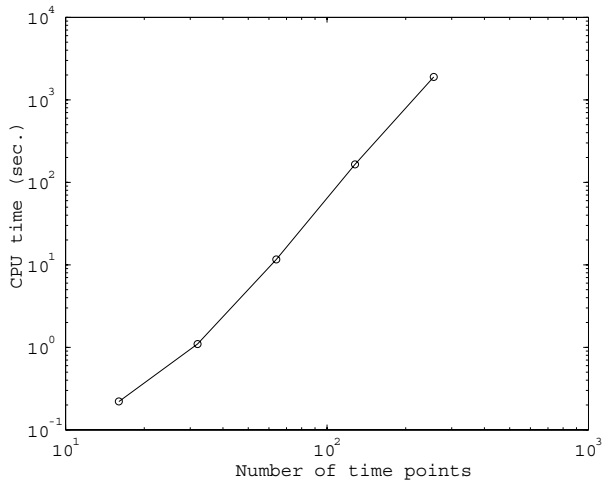


Fig. 7. CPU time as a function of N

Numerical results

The analysis contained in the previous section shows that windowing can improve significantly the simulation results, in terms of both accuracy and appearance of the computed spectrum. This is illustrated by the following example, in which the spectrum obtained directly from (10) (i.e. using the rectangular window) is compared with the spectrum obtained by applying the Blackmann window of length $2N + 1$ to $\{\Delta \mathbf{x}(t_k)\}$.

Fig. 6 shows a CMOS optical amplifier. This circuit amplifies the output of a photodetector, modeled by a current source applied to its input. The amplifier load is modeled by a 30 k Ω resistor at the amplifier's output. A signal having a uniform power spectral density within a 1 GHz bandwidth (white noise) was applied to the amplifier's input, and the spectrum of the output signal was

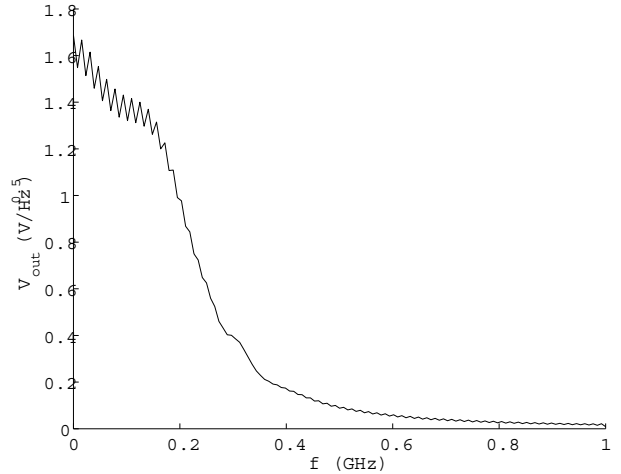


Fig. 8. Output spectrum, rectangular window

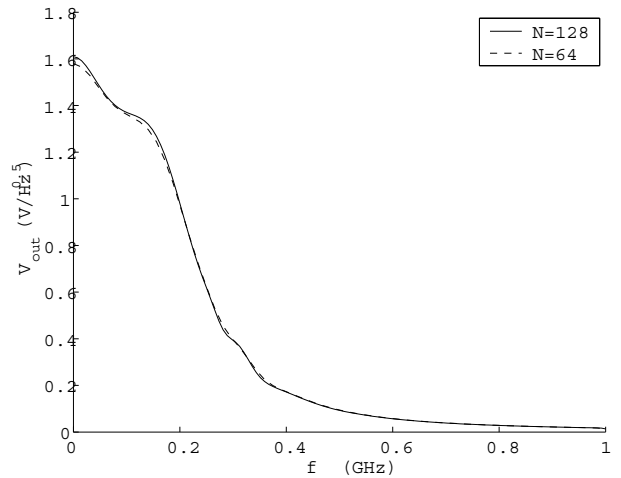


Fig. 9. Output spectrum, Blackmann window

computed using the algorithm described earlier, with various values of N . The CPU time required for simulation on a Sun Ultra 60 workstation running Solaris 8 is shown in Fig. 7 as a function of N . The slope of the line indicates that the CPU time grows approximately as N^3 ; for $N = 128$, it was approximately 32 minutes.

The spectrum of the output signal obtained directly from (10) for $N = 128$ is shown in Fig. 8; the ripple caused by the Gibbs phenomenon is clearly visible in the graph. Fig. 9 shows the spectrum obtained by applying the Blackmann window, with $N = 128$, to the simulation results. For comparison purposes, the graph corresponding to $N = 64$ (both for simulation and windowing) is also shown. No spurious oscillations are visible in either graph, thanks to the high attenuation (approximately 70 dB) of the side lobes in the Blackmann window's error kernel. It can also be seen that the two values of N

give almost identical results: the largest difference (approximately 2%) occurs at $f = 0$. This is consistent with the observation made earlier that appropriate windowing reduces the error in the results, and thus the value of N necessary to attain a given accuracy.

Conclusion

The approach to frequency-domain simulation described in this paper is, in a way, the dual of the well-known analysis method based on harmonic balance, in that the unknown signals are expanded in a sinusoidal series in the frequency domain, instead of the time domain. Taking the inverse Fourier transform of the series expansion transforms the differential equation describing the system into a finite set of algebraic equations in the time domain. Just as in harmonic balance, the number of equations is chosen based on the desired accuracy. Unlike harmonic balance, however, the algorithm described in this paper is suitable for handling signals with continuous spectra. Using the algorithm on even very simple circuits reveals that the Gibbs phenomenon causes a degradation in the simulation results. This observations leads naturally to investigating the use of windowing techniques for the purpose of improving the simulation results. It has been shown that the error introduced by windowing is related by a very simple expression (a convolution integral) to $K_W(\hat{\omega})$, which for this reason has been named the windowing error kernel. Because of this simple relationship, an analysis based on $K_W(\hat{\omega})$, instead of the more commonly used $W(\hat{\omega})$, is more suitable to examine the features of a given window, such as its resolution or the creation of spurious oscillations. Numerical results confirm the theoretical analysis, and indicate that the algorithm described in this paper, when combined with windowing, can be an effective tool for the simulation of nonlinear systems in the presence of continuous-spectrum signals. As with harmonic balance, the computational effort required for the analysis increases with the desired accuracy: in this case, the resolution in the computed spectrum. This is due mostly to the increase in the size of the system of equations that must be solved. For this reason, the use of algorithms to solve systems of equations that do not require matrix decompositions will be investigated.

References

- [1] K. S. Kundert, "Introduction to RF simulation and its application," *IEEE J. Solid-State Circuits*, vol. 34, pp. 1298–1319, Sept. 1999.
- [2] A. Demir, E. W. Y. Liu, and A. L. Sangiovanni-Vincentelli, "Time-domain non-Monte Carlo noise simulation for nonlinear dynamic circuits with arbitrary excitations," *IEEE Trans. Computer-Aided Design*, vol. 15, pp. 493–505, May 1996.
- [3] M. Okumura, H. Tanimoto, T. Itakura, and T. Sugawara, "Numerical noise analysis for nonlinear circuits with a periodic large signal excitation including cyclostationary noise sources," *IEEE Trans. Circuits Syst. I*, vol. 40, pp. 581–590, Sept. 1993.
- [4] J. Roychowdhury, D. Long, and P. Feldmann, "Cyclostationary noise analysis of large RF circuits with multitone excitations," *IEEE J. Solid-State Circuits*, vol. 33, pp. 324–336, Mar. 1998.
- [5] R. Telichevesky, K. S. Kundert, and J. White, "Efficient AC and noise analysis of two-tone RF circuits," in *Proc. 33rd Design Automation Conf.*, pp. 292–297, June 1996.
- [6] K. S. Kundert and A. Sangiovanni-Vincentelli, "Simulation of nonlinear circuits in the frequency domain," *IEEE Trans. Computer-Aided Design*, vol. CAD-5, pp. 521–535, Oct. 1986.
- [7] K. S. Kundert, J. White, and A. Sangiovanni-Vincentelli, *Steady-State Methods for Simulating Analog and Microwave Circuits*. Norwell, MA: Kluwer Academic Publishers, 1990.
- [8] V. Rizzoli and A. Neri, "State of the art and present trends in nonlinear microwave CAD techniques," *IEEE Trans. Microwave Theory Tech.*, vol. 36, pp. 343–365, Feb. 1988.
- [9] A. V. Oppenheim and R. W. Schaffer, *Discrete-Time Signal Processing*. Englewood Cliffs, NJ: Prentice Hall, 1989.
- [10] F. J. Harris, "On the use of windows for harmonic analysis with discrete Fourier transform," *Proc. IEEE*, vol. 66, pp. 51–83, Jan. 1978.